ADVANCED HEALTHCARE MATERIALS
www.advhealthmat.de

Modulating the Selectivity and Stealth Properties of Ellipsoidal Polymersomes through a Multivalent Peptide Ligand Display

*Kristel C. Tjandra, Chelsea R. Forest, Chin Ken Wong, Sheilajen Alcantara, Hannah G. Kelly, Yi Ju, Martina H. Stenzel, Joshua A. McCarroll, Maria Kavallaris, Frank Caruso, Stephen J. Kent, and Pall Thordarson**

There is a need for improved nanomaterials to simultaneously target cancer cells and avoid non-specific clearance by phagocytes. An ellipsoidal polymersome system is developed with a unique tunable size and shape property. These particles are functionalized with in-house phage-display cell-targeting peptide to target a medulloblastoma cell line in vitro. Particle association with medulloblastoma cells is modulated by tuning the peptide ligand density on the particles. These polymersomes has low levels of association with primary human blood phagocytes. The stealth properties of the polymersomes are further improved by including the peptide targeting moiety, an effect that is likely driven by the peptide protecting the particles from binding blood plasma proteins. Overall, this ellipsoidal polymersome system provides a promising platform to explore tumor cell targeting in vivo.

1. Introduction

In the last 40 years, the field of nanomedicine has made many strides toward making drug therapies more potent, more selective, and most importantly less toxic. There are several nanomedicine therapies already in the market such as Doxil,[1] a liposomal formulation of doxorubicin, Abraxane,[2] an albumin-bound paclitaxel nanoparticle, and NanoTherm,[3] an iron oxide nanoparticle.[4] These therapies have shown improved pharmacokinetics, biodistribution, and better drug tolerance compared to the free drug. However, the extensive area of nanoparticle characteristics, such as size, shape, active-cell targeting, as well as chemical properties that can be manipulated has not been exhausted, leaving a large room for improved nanoparticle synthesis for efficient drug delivery.

Both nanoparticle shape and their ligand density have been suggested to play a major role in effective drug delivery.[5–7] While most earlier studies have been done on spherical nanoparticles, recent work have suggested that nanoparticle shape can affect their cellular uptake, biodistribution, and cytotoxicity.[8,9] The circulating explanation is that the higher aspect ratio of non-spherical particles and their geometrical orientations allows for

Dr. K. C. Tjandra, C. R. Forest, Dr. C. K. Wong, Prof. M. H. Stenzel, Prof. P. Thordarson
School of Chemistry
The University of New South Wales
Sydney, NSW 2052, Australia
E-mail: p.thordarson@unsw.edu.au

Dr. K. C. Tjandra, C. R. Forest, Dr. C. K. Wong, Dr. J. A. McCarroll, Prof. M. Kavallaris, Prof. P. Thordarson
Australian Centre for Nanomedicine
The University of New South Wales
Sydney, NSW 2052, Australia

Dr. K. C. Tjandra, C. R. Forest, Dr. C. K. Wong, S. Alcantara, H. G. Kelly, Dr. Y. Ju, Dr. J. A. McCarroll, Prof. M. Kavallaris, Prof. F. Caruso, Prof. S. J. Kent, Prof. P. Thordarson
ARC Centre of Excellence in Convergent Bio-Nano Science and Technology
Australia

S. Alcantara, H. G. Kelly, Prof. S. J. Kent
Department of Microbiology and Immunology
The University of Melbourne at the Peter Doherty Institute for Infection and Immunity
Parkville, VIC 3000, Australia

Dr. Y. Ju, Prof. F. Caruso
Department of Chemical Engineering
The University of Melbourne
Parkville, VIC 3010, Australia

Prof. M. H. Stenzel
School of Chemistry
Centre for Advanced Macromolecular Design (CAMD)
The University of New South Wales
Sydney, NSW 2052, Australia

Dr. J. A. McCarroll, Prof. M. Kavallaris
Translational Cancer Nanomedicine Theme
Children's Cancer Institute
Lowy Cancer Research Centre
The University of New South Wales
Sydney, NSW 2031, Australia

Dr. J. A. McCarroll, Prof. M. Kavallaris
School of Women's and Children's Health
Faculty of Medicine
The University of New South Wales
Sydney, NSW 2052, Australia

The ORCID identification number(s) for the author(s) of this article can be found under https://doi.org/10.1002/adhm.202000261

DOI: 10.1002/adhm.202000261

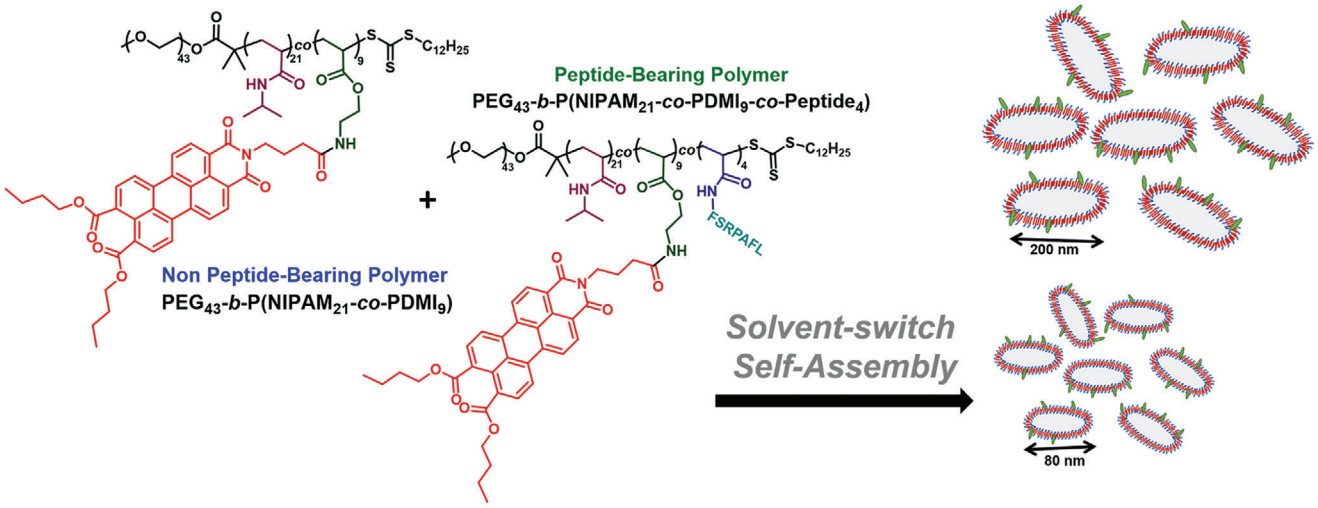

Scheme 1. Structures of the block copolymers used for the solvent-switch self-assembly formation of multivalent polymersomes bearing medulloblastoma cell-targeting peptides.

an increased interaction with cell surface receptors and offers a more diverse cellular mode of entry.[10–12] However, the extent to which particle geometry contribute to specific biological effects were still debatable, thus highlighting the need for further investigations. Our current study gives insight into the effect of ligand density on targeting using a non-spherical polymersome platform.

Polymersomes are artificial vesicles with a bilayer membrane, made up of amphiphilic block copolymers. This bilayer system is desirable for drug delivery as it allows the versatility of imbedding hydrophobic drugs in the core of the membrane or a hydrophilic drug to be encapsulated within the aqueous core of the particle.[13–15] One of the advantages polymersomes have over other nanoparticles is that they can easily adopt several morphologies apart from spherical such as rod-like, ellipsoidal, and disc using several different techniques without the need for post assembly manipulation or scaffolds like particle replication in non-wetting templates.[16–18]

One downfall of many nanoparticle based therapeutic systems is the rapid clearance from the blood by phagocytes that leads to poor tumor biodistribution and pharmacokinetics. This rapid clearance is mainly due to blood protein interactions with the surface of the nanoparticle which leads to increased immune cell association.[19] One approach to evade this large scale immune clearance is by precoating particles with polyethylene glycol (PEG) to create a stealthy profile. Here we aim to determine if the presence of a cell-targeting peptide on the surface of the particle changes the immune cell-association of the particle and therefore predicting their clearance from the blood.

Herein we report for the first time the synthesis of a selective and multivalent polymersome system using two block-copolymers (**Scheme 1**). We investigated the effect of varying cell-targeting peptide density and particle size on both the selectivity of non-spherical polymersomes toward tumor cells and their stealth property toward primary human immune cells. A suite of 15 ellipsoidal polymersomes (**Table 1**) were reproducibly generated building on our previous work on self-assembled perylene-bearing polymer system.[16,20] Ten of these polymersomes will be referred to as the low-ligand density (LLD) polymersomes consisting of 5 ± 80 nm (major axes) particles and 5 ± 400 nm (major axes) particles with varying peptide ligand densities. The remaining five particles are the high-ligand density (HLD) ± 100 nm (major axes) particles. The perylene moiety provides the necessary hydrophobicity and liquid crystallinity for the polymer to self-assemble into its anisotropic shape while serving as a highly stable fluorescent component that is convenient for in vitro imaging.[21] These polymersomes were functionalized with a heptapeptide FSRPAFL, which we discovered through a peptide phage-display library as having selectivity and high binding

Table 1. Hydrodynamic diameter and polydispersity indices of small and large high ligand density (HLD) and low ligand density (LLD) polymersomes in this study as determined through dynamic light scattering (DLS) measurements.

Size groups		Peptide ligand density (equivalent peptide units)	*Z*-average (D_h [nm])[a]	PdI[a]
Small	HLD	0% (0)	96 ± 0.5	0.22 ± 0.01
		25% (1)	68 ± 0.8	0.263 ± 0.02
		50% (2)	86 ± 0.2	0.25 ± 0.02
		75% (3)	91 ± 0.8	0.11 ± 0.02
		100% (4)	109 ± 0.1	0.112 ± 0.03
	LLD	0% (0)	70 ± 0.3	0.16 ± 0.01
		25% (0.375)	69 ± 0.4	0.12 ± 0.00
		50% (0.75)	72 ± 0.4	0.13 ± 0.01
		75% (1.125)	70 ± 0.6	0.10 ± 0.02
		100% (1.5)	70 ± 1.3	0.15 ± 0.05
Large		0% (0)	201 ± 1.2	0.14 ± 0.01
		25% (0.375)	191 ± 0.9	0.11 ± 0.03
		50% (0.75)	196 ± 1.1	0.14 ± 0.01
		75% (1.125)	197 ± 2.0	0.14 ± 0.03
		100% (1.5)	193 ± 4.5	0.14 ± 0.05

[a] D_h and PdI = average ± standard deviation (the approximate magnitude of errors of the particles' hydrodynamic diameter were automatically generated by the Zetasizer Nano instrument based on three independent scans).

affinity against human medulloblastoma (DAOY) cells.[22] The stealth property of these ellipsoidal polymersomes was determined through their association and clearance by human phagocytes and compared against a known "stealthy" PEG-based particle by incubating the particles with whole human blood.[23]

We hypothesized that the higher peptide ligand density will give greater selectivity to these polymersomes and that the peptide will not alter their-like stealth property. Our results showed that indeed the higher ligand density particles were more selective. More interestingly, this increase was greatly enhanced when a certain ligand density threshold was reached. Further, the addition of the medulloblastoma cell-targeting peptide also markedly improved the stealth property of these particles.

2. Results and Discussions

2.1. Polymer Synthesis and Characterization

Poly(ethylene glycol)-*block*-poly(*N*-isopropylacrylamide-*co*-perylene diester monoimide) (PEG_{43}-*b*-P($NIPAM_{21}$-*co*-$PDMI_9$)) polymer, which was derived from PEG_{43}-*b*-P($NIPAM_{21}$-*co*-*t*-$BocAEA_9$) was synthesized according to our previously reported protocol.[20,24] The first step in the synthesis of PEG_{43}-*b*-P($NIPAM_{21}$-*co*-*t*-$BocAEA_9$) involved the copolymerization reaction between two monomers: 1) *N*-isopropylacrylamide (NIPAM) and 2) *tert*-butyloxycarbonyl-aminoethyl acrylate (*t*-BocAEA), using a reversible addition-fragmentation chain transfer (RAFT) polymerization technique in the presence of PEG_{43}-modified trithiocarbonate macro-RAFT agent. The use of *t*-Boc-aminoethyl acrylate (*t*-BocAEA) was a convenient way to pre-install a protected primary amine functionality as a handle for the perylene moiety, which acts both as a fluorescent probe and to direct the self-assembly of the polymers toward non-spherical polymersomes. The perylene was added to the polymer block in the form of an *N*-(pentafluorophenyl butyl ester)-perylene-3,4,9,10-tetracarboxylic monoimide dibutyl ester (PDMI-PFP).[20] Here, the *t*-Boc protecting group was used to avoid cleavage of the RAFT trithiocarbonate moiety by the primary amine during RAFT polymerization (Scheme S1, Supporting Information).

To facilitate the peptide ligand attachment, a diblock copolymer, namely poly(ethyleneglycol)-*block*-poly(*N*-isopropylacrylamide-*co*-*N*-(*tert*-butoxylcarbonyl) aminoethyl acrylate-*co*-pentafluorophenyl ester acrylate) (PEG_{43}-*b*-P($NIPAM_{21}$-*co*-*t*-$BocAEA_9$-*co*-PFP_4)) was synthesized via RAFT polymerization following modifications to previously reported procedures (Scheme S1, Supporting Information).[20,25] The design of this polymer was intended to provide an orthogonal handle for the incorporation of two distinct functionalities. The first component was the previously mentioned perylene moiety, which was reacted with the amino group of the block copolymer, and the second moiety was a heptapeptide (as a targeting ligand) which was attached through a reaction with the pentafluorophenyl ester group via the *N*-terminus. The success of these syntheses and the degree of polymerization was confirmed and determined using ^{1}H NMR spectroscopy and dimethylacetamide (DMAc) gel permeation chromatography (Figure S1, Supporting Information).

Heptapeptide FSRPAFL, which was previously described to have selectivity toward our target medulloblastoma cell line (DAOY),[22] was conjugated onto the PEG_{43}-*b*-P($NIPAM_{21}$-*co*-*t*-$BocAEA_9$-*co*-PFP_4) polymer backbone using a diisopropylethylamine base in *N,N*-dimethylformamide for 48 h at 40 °C. To synthesize the LLD polymer, only 1.5 molar equivalent of this peptide was reacted onto the polymer backbone, which contains four repeating units of pentafluorophenol—as indicated by the ^{1}H NMR (Scheme S2, Supporting Information). Six molar equivalents of the heptapeptide was reacted with the polymer in a similar manner to create a polymer with HLD. This synthesis strategy allows a fine-tuning of the peptide units on the polymer backbone (with 0, 0.375, 0.75, 1, 1.125, 1.5, 2, 3, or 4 equivalent peptide units per polymersome). The progress of the conjugation reaction was monitored qualitatively using ^{19}F NMR, where the gradual decrease in the broad polymeric pentafluorophenyl signal was indicative of the extent of conjugation (**Figure 1**).

The ^{19}F NMR spectra of the crude reaction mixture for the LLD polymer at 24 h post reaction showed signals from the fluorine of the pentafluorophenol group. The broad singlet peaks at δ −152, −157, and −162 ppm (Figure 1, signals a, b, and c), suggested that the polymer-bound pentafluorophenyl was still present, and hence incomplete conjugation. Sharp signals at δ −168, −171, and −185 ppm were indicative of free pentafluorophenol, indicating that some conjugation had occurred (Figure 1, signals d, e, and f). Thus, the reaction was left for another 24 h. At 48 h, the ^{19}F NMR spectra suggested that the proportion of polymer-bound pentafluorophenyl had been reduced, but not completely (Figure 1).

It was important to ensure that no free pentafluorophenyl groups were left on the polymer backbone, as cross-linking with the free amine on the amino-ethyl ester amine would impede subsequent attachment of the PDMI-PFP. Hence, in order to fully substitute the pentafluorophenol group, propargylamine was added into the reaction mixture as a less-hindered primary amine and stirred for a further 24 h. The disappearance of the broad singlet peaks (labeled a–c in Figure 1) suggested that there were no polymer-bound pentafluorophenyl moieties left on the LLD polymer backbone (Figure 1C). The absence of this fluorine signal indicated that the reaction between the pentafluorophenyl ester and the free amine of the linear peptide did occur. Hence, the targeting peptides were successfully conjugated to the polymer backbone.

The HLD polymer, on the other hand, did not require the additional propargylamine capping step described above. After 72 h reaction with the six molar equivalents of peptide, the ^{19}F NMR spectra showed no unreacted pentafluorophenol groups left on the HLD polymer backbone (Figure S2, Supporting Information). The reaction products were dialyzed to remove any unreacted peptides and free pentafluorophenol. This procedure was followed by the deprotection of the *tert*-butylcarbonyl (*t*-Boc) moiety to produce free amines, which upon conjugation with the *N*-(pentafluorophenyl butyl ester)-perylene-3,4,9,10-tetracarboxylic monoimide dibutyl ester (PDMI-PFP) yielded the final polymer products. Successful attachment of the perylene moiety onto the polymer backbones was confirmed using ^{1}H–^{13}C 2D NMR (Figure S3, Supporting Information). However, signals corresponding to protons on the peptide moiety could not be assigned due to poor resolution (Figure S3, Supporting Information).

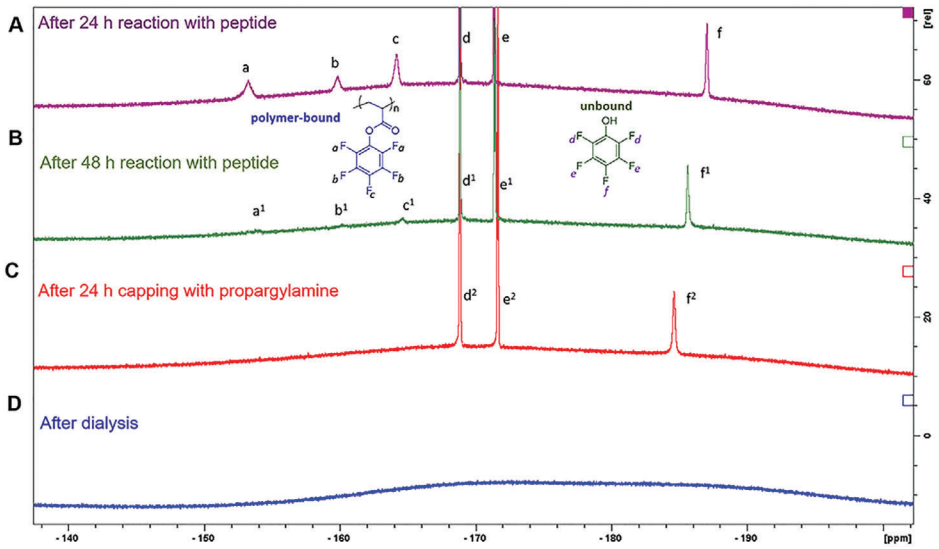

Figure 1. ^{19}F NMR spectra of the progression of low density peptide functionalization and propargylamine capping onto PEG_{43}-*b*-P($NIPAM_{21}$-*co*-*t*-$BocAEA_9$-*co*-PFP_4) in $CDCl_3$. ^{19}F NMR trace: A) after 24 h reaction with FSRPAFL peptide; B) after 48 h reaction with peptide; C) after 24 h capping with propargylamine, showing the disappearance of a–c peaks; and D) after dialysis against dichloromethane and ethanol.

2.2. Polymersome Formation and Characterization

Ellipsoidal polymersomes in this study were formed through a solvent-switch method with tetrahydrofuran as the good solvent and water as the antisolvent (**Figure 2**A).[16,20,26,27] The solubility of non-peptide bearing block copolymer PEG_{43}-*b*-P($NIPAM_{21}$-*co*-$PDMI_9$) was different from that of its peptide-bearing counterparts. While block copolymer PEG_{43}-*b*-P($NIPAM_{21}$-*co*-$PDMI_9$) dissolved reasonably well in tetrahydrofuran, block copolymer, PEG_{43}-*b*-P($NIPAM_{21}$-*co*-$PDMI_9$-*co*-$Peptide_{1.5(LLD)\ or\ 4(HLD)}$), did not. Therefore, in order to create a homogeneous solution, the peptide-bearing polymers were dissolved in *N,N*-dimethylformamide (10% of the final volume), prior to dilution with tetrahydrofuran. Water was then added to the polymer solution at a constant volume (in this case, 500 µL), triggering aggregation and self-assembly. The tetrahydrofuran solvent was evaporated slowly over 16 to 20 h yielding ellipsoidal polymersomes in water (Figure 2A). The *N,N*-dimethylformamide solvent leftovers in the peptide-bearing polymersomes was removed by dialysis against water.

2.3. Tuning the Ligand Density of the Polymersomes

Ligand density of the peptide on the surface of polymersomes was tuned by blending the non-peptide and peptide-bearing polymers during polymersome formation (step 1, Figure 2A). The total mass of both polymers (i.e., 0.5 mg) was kept constant across all samples. For ease of discussion, these polymersomes are referred according to their sizes (small or large), and the composition of peptide-bearing block copolymers PEG_{43}-*b*-P($NIPAM_{21}$-*co*-$PDMI_9$-*co*-$peptide_{1.5(LLD)\ or\ 4(HLD)}$) beginning from 0, 25, 50, 75, to 100%. In the case of 0%, the polymersome was formed with only the non-peptide polymer, while the 100% samples were made out of only the peptide-bearing polymer (≈4 equivalent or units of peptides per polymer).

2.4. Tuning the Size of Polymersomes

Previous work in the group has found that polymersome sizes of this specific system can be tuned by adjusting the volume of tetrahydrofuran during formation.[20] Two different volumes were chosen in this study (i.e., 500 and 800 µL) to yield polymersomes with hydrodynamic diameters of ≈70 nm and ≈200 nm, as confirmed by dynamic light scattering (DLS) (Figure S4, Supporting Information; Table 1). Due to the ellipsoidal nature of the polymersomes, DLS can only provide a rough estimate of the hydrodynamic diameter (D_h) of these polymersomes. This discrepancy is due to the spherical geometry (hard spheres) that is assumed in the measurement process, hence discounting the possible rotational diffusion (tumbling motion) of these particles in solution.[28] A more accurate measurement (including the major/minor axes and aspect ratio) of these polymersomes was determined by taking transmission electron microscopy (TEM) images and using ImageJ analysis (Figures S5–S7, Supporting Information).

Here the TEM images of the particles showed that the addition of the peptide units onto the polymer backbone did not alter the shape of the resulting polymersomes. This observation suggests that the peptide did not disrupt the liquid crystallinity of the particle. Note that the DLS measurements of the polymersomes sizes did not correlate to the TEM image analyses (using ImageJ) in relation to large polymersomes (Figure S6, Supporting Information) compared to the small polymersomes (Figure S5, Supporting Information). The major axes of the large polymersomes as determined from the from transmission electron microscopy (TEM) images indicated that they were 404 ± 64 nm in size (as opposed to 194 ± 2.1 nm as indicated by DLS). On the other hand, the hydrodynamic size of the small polymersomes according to the DLS measurement (70 ± 0.6 nm) was a closer match to the major axes (80 ± 12 nm) indicated by the TEM images (Figure 2B,C).

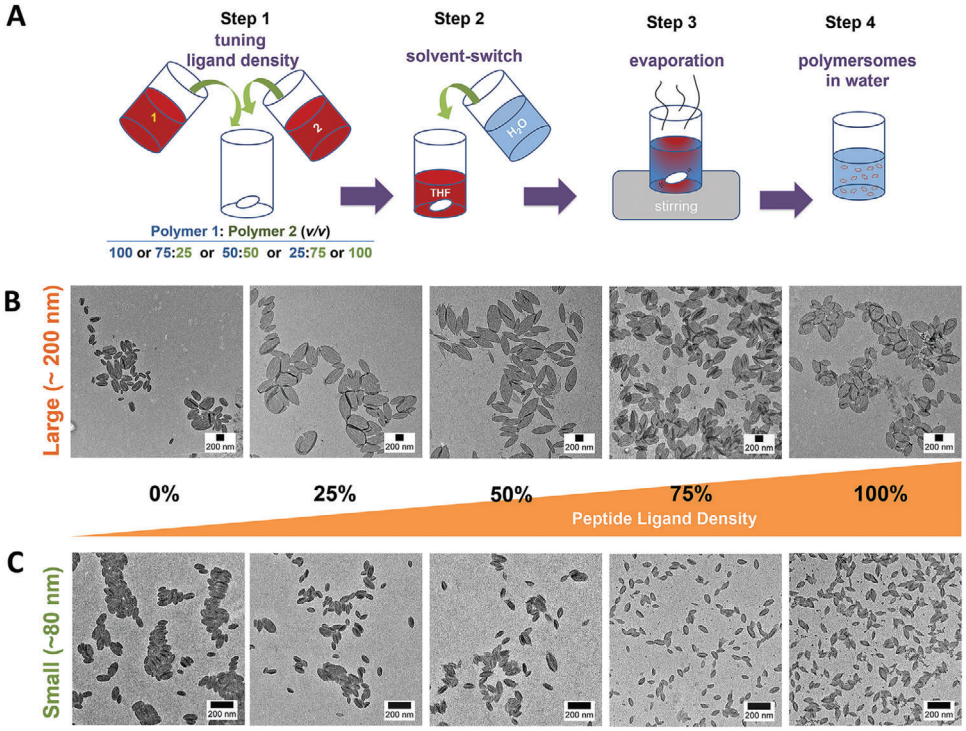

Figure 2. Polymersome formation using a solvent-switching method. A) PEG_{43}-*b*-P($NIPAM_{21}$-*co*-$PDMI_9$ polymer (1) and PEG_{43}-*b*-P($NIPAM_{21}$-*co*-$PDMI_9$-*co*-$peptide_{1.5\ (LLD)\ or\ 4\ (HLD)}$ polymer (2) were dissolved in THF (in red). Addition of water (in blue) induces self-assembly of the polymer. Different ratios of PEG_{43}-*b*-P($NIPAM_{21}$-*co*-$PDMI_9$ and PEG_{43}-*b*-P($NIPAM_{21}$-*co*-$PDMI_9$-*co*-$peptide_{1.5/4}$ polymer mixture in "Step 1" are key in tuning the ligand density of the polymersome, while the increasing volume of THF corresponds to an increase in resulting polymersome sizes. B,C) TEM images of the two polymersome populations (small and large low-ligand density (LLD) polymersomes) of varying peptide ligand-density (expressed in percentage). Peptide ligand density on polymersomes is indicated by the percent value: 0% for polymersomes made of non-peptide PEG_{43}-*b*-P($NIPAM_{21}$-*co*-$PDMI_9$) polymer only, and 100% for polymersomes made of PEG_{43}-*b*-P($NIPAM_{21}$-*co*-$PDMI_9$-*co*-$peptide_{1.5}$). Scale bars: 200 nm.

These differences in sizes from the two techniques indicated that the sizes of the larger polymersomes were underestimated by the DLS. Despite this inconsistency, DLS is still a useful tool for checking particle dispersity in solution (expressed in terms of a polydispersity index, PdI) as an indication of their size distributions.[28] Using these two polymers and by adjusting the tetrahydrofuran volumes, two populations of ellipsoidal polymersomes according to their sizes, having varying ligand densities were successfully generated. The stability of these polymersomes in the cell culture media and at pH ranging from 3–8 was confirmed (Figure S16, Supporting Information).

2.5. Active Transport of Polymersomes into Medulloblastoma Cells

The effect of varying the peptide ligand density and particle sizes on the uptake of the polymersomes inside the medulloblastoma cells (DAOY) was investigated by flow cytometry. We previously reported a detailed characterization of the targeting peptide (FSPRPAFL) used for functionalizing these polymersomes and showed that the peptide is capable of mediating a ligand-mediated endocytosis.[22] Herein we confirm that such metabolically active mechanism was also responsible for the transport of the polymersomes into the target cells. In brief, DAOY cells were seeded onto tissue culture plates and incubated with 0.025 mg mL^{-1} of low-ligand density polymersomes at 37 and 4 °C for 2 h (concentration was chosen according to the maximum tolerated concentration tested, see Figure S8, Supporting Information). Note that 0.025 mg mL^{-1} concentration of the HLD polymersomes was toxic for the cells at 72 h. However, this concentration is well tolerated by the cells within 2 h post-incubation as demonstrated by cytotoxicity assays (see Figure S8C, Supporting Information). Hence, the cellular uptake study proceeded with this concentration. After removal of the polymersomes, the cells were washed with phosphate saline buffer, trypsinized, and harvested for flow cytometry analysis using methods previously described.[22] The fluorescent intensities were corrected for the differences observed in each sample (Figure S9, Supporting Information). Single cell populations were sorted using flow cytometry. The median fluorescence intensity of the polymersome-incubated cells was indicative of the concentration of polymersomes that were internalized by the cells as demonstrated by confocal microscopy (Figure S10, Supporting Information).

It was observed that at 4 °C (at which cells remained viable but metabolically inactive),[29,30] minimal cellular uptake was achieved as indicated by the baseline fluorescence intensity of the single cells across the ten different polymersome samples (small and large, 0% to 100% peptide ligand density). This was not the case at a physiological temperature of 37 °C, where the increase in peptide density was associated to an increase in cellular uptake as indicated by the increase in the detected fluorescence

intensity. The cellular internalization of the polymersomes was inhibited at 4 °C (according to a paired *t*-test comparing the samples at both temperatures, p (two-tailed) = 0.000005. This suggested that these polymersomes were taken up by the cells via a metabolically energy-dependent process rather than passive membrane diffusion (Figure S11, Supporting Information).

2.6. Comparing Polymersome Cellular Association in Non-Target Cells

A key function we aimed to demonstrate with these polymersomes was selectivity toward their target cancer cell through the addition of a medulloblastoma cell-targeting peptide (in this case, peptide FSRPAFL). The selectivity of the polymersomes toward the target medulloblastoma cell line, DAOY, was assessed by comparing their cellular associations for non-target cells (HEK293). A cellular association study using flow cytometry was performed comparing the fluorescence intensity of cells treated with the same concentration of the polymersomes solution in cell culture media. The HEK293 cell line, which is a human embryonic kidney cell line with similar characteristics to neuronal cells was used as the control non-target cell line.[31]

Interestingly, according to the flow cytometry measurement on the LLD polymersomes the non-liganded polymersomes associated more to the target cells, DAOY, compared to the non-target cells, HEK293 (0% peptide polymersome samples, both small and large, $p = 0.000014$ for large polymersome and $p = 0.000045$ for small polymersomes) (**Figure 3**). The addition of the peptide onto the polymersomes led to an incremental nanoparticle uptake into DAOY cells. Notably, the same effect was not observed in the HEK293 cells, where the presence of the peptide ligand on both the small and the large polymersomes did not alter the cellular uptake of these particles. This finding indicates that the increase in peptide-ligand density on the polymersomes surface led to the increased selectivity of these polymersomes toward the target tumor cells compared to the control non-tumor cells.

The cellular association pattern of the small LLD polymersomes was very similar to the HLD polymersomes at 37 °C except for the 100% small polymersomes where a significant difference was observed (**Figure 4**). The degree of association of the 100% peptide-bearing polymersome, as indicated by the median fluorescence intensity of the particles, was almost three times higher for the small HLD polymersomes compared to the small LLD polymersomes. This stark increase in cellular association suggests that an enhanced interaction was achieved once a high peptide ligand density threshold (in this case, 4 peptide units per polymersomes) was reached.[32] Interestingly, the same phenomenon was not observed in two different non-target cell lines (HEK293 and HBEC5i) (Figure 4A,B), which demonstrated that the multivalent binding was a cell-specific event.

The observed enhancement in binding and selectivity toward the DAOY cells over the non-target non-tumor cells can be explained based on the latest understanding of multivalent targeting of cell-receptors.[32] In particular the work of Frenkel and co-workers on the concept of selectivity in multivalency helps explains the results here.[33,34] In short, while overall binding strengths might be expected to increase somewhat linearly with the number of interacting ligands (here the peptide) on the nanoparticles, the selectivity between cells with many target receptors (here DAOY) and those with fewer receptors (the non-targeting, HEK293 and HBEC5i) will be highly non-linear. This is consistent with there being a threshold concentration of ligands, above which the interaction of the nanoparticle becomes much stronger for the cell lines with many target receptors than those cell lines with fewer receptors (compare the uptake at 100% ligand density in Figure 4A with Figure 4B). Multivalent systems that show such selectivity are also usually characterized by very steep (sigmoidal) non-linear increase in the bound fraction of ligands toward their target cell line once a certain threshold concentration of ligands has been

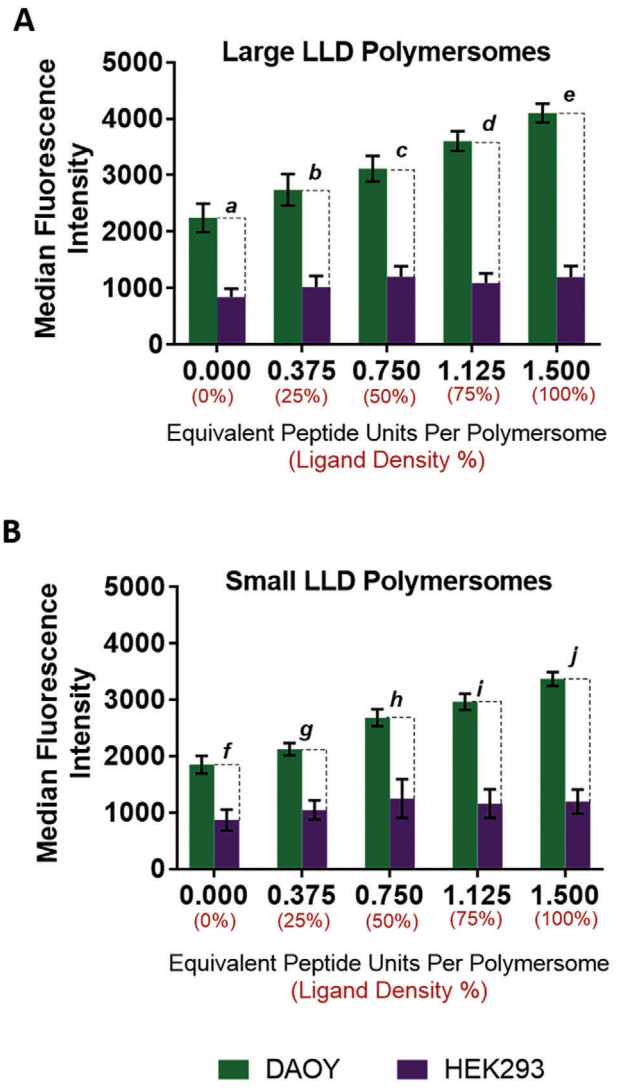

Figure 3. Representative graph of the flow cytometry measurements for comparing the cellular association of A) large versus B) small LLD polymersomes in DAOY and HEK293 cells. The difference in the median fluorescence intensity (MFI) of DAOY and HEK293 (i.e., MFI_{DAOY}–MFI_{HEK293}) is represented by the dashed lines (—). Two-way ANOVA, Tukey's multiple comparison tests, were calculated for the difference in the MFI of these two cell lines, for a, $p = 0.000014$; b, $p = 0.000003$; c, $p = 0.000001$; d, $p = 0.00000008$; e, $p = 0.00000004$; f, $p = 0.000045$; g, $p = 0.000022$; h, $p = 0.0000027$; i, $p = 0.0000003$; and j, $p = 0.00000006$. Error bars represent standard error of the mean ($n = 3$).

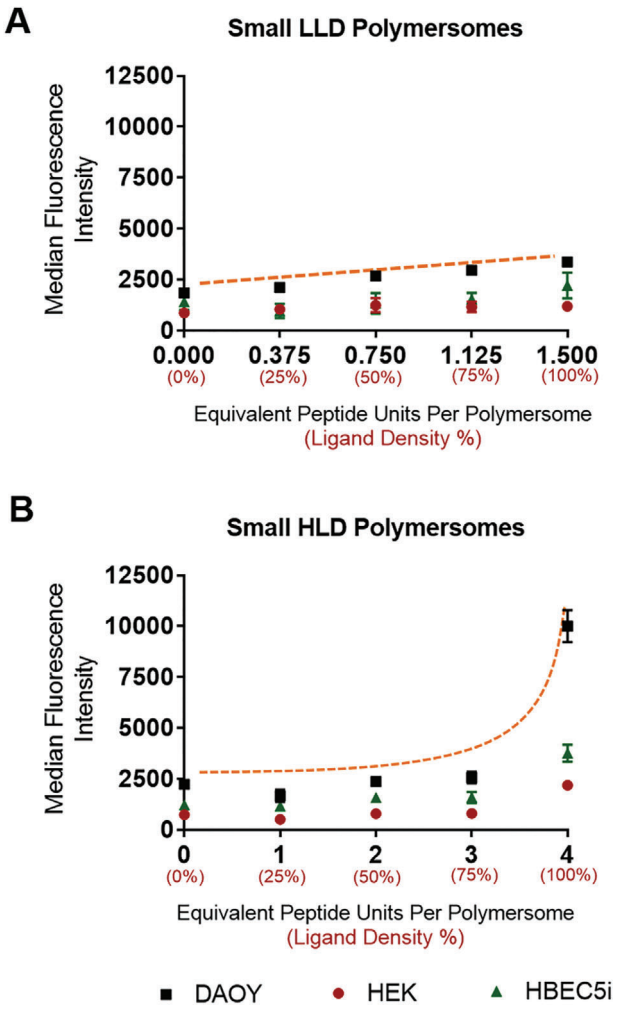

Figure 4. Representative graphs of the flow cytometry measurements for comparing the uptake of small HLD and LLD polymersomes in DAOY, HEK293, and HBEC5i cells (a human brain microvascular endothelial cell line). A) Low ligand density (LLD) polymersomes with the 0–1.5 equivalent peptide units corresponding to 0 to 100% ligand density, B) high ligand density (HLD) polymersomes with the 0–4 equivalent peptide units corresponding to 0 to 100% ligand density. Each data point indicates the median fluorescence intensity (MFI) of the detected polymersomes signal. Error bars represent standard error of the mean ($n = 3$).

reached. Here it appears that this threshold concentration, which resulted in a more optimal interaction with the target cell, corresponds to the 100% HLD ligand concentration (equivalent to 4 peptides per polymersome).

Overall, the selectivity of the polymersome was more pronounced in polymersomes with higher peptide ligand density. This was especially true for the 100% high ligand density small polymersomes where a threefold increase in association was observed (as referred to in Figure 4). Comparisons of polymersomes cellular uptake in DAOY, HEK293, and HBEC5i cells suggested that the polymersomes in general associate more with the target cell (DAOY). We also found that the size of the polymersomes was, in this case, less of a factor in the selectivity of these polymersomes (as indicated in Figure 3).

2.7. Stealth Characteristics of Peptide-Bearing Polymersomes in Human Blood

Next, we evaluated the effect of the tumor cell-targeting peptide attached to the small HLD polymersomes and its potential association with human blood immune cells by flow cytometry (**Figure 5**A). We studied the small HLD polymersomes in comparison to an alternate PEG-based particle we have previously developed.[23] We found that the non-peptide bearing polymersomes had a similar and low level of association with blood phagocytes (monocytes and granulocytes) as the PEG particles, although a higher level of association with B cells was observed (Figure 5A). The association of particles with B cells is an effect commonly driven by association of the particles with complement in plasma and complement receptors found on the surface of B cells.[35]

We were concerned that the addition of the peptide ligand to the PEG based polymersomes could interfere with the hydrophobicity of the particles and reduce the stealth-like properties of the particle, as previously observed with antibody labeled particles.[36] However, we observed the opposite, with the highest ligand density polymersomes having reduced association with neutrophils (granulocytes), monocytes, and B cells which we speculate was due to the protective nature of the cancer cell-targeting peptide against binding to human blood plasma proteins (Figure 5B).

The reduced association of the peptide-targeted polymersomes and B cell association observed in the whole human blood assay suggested the possibility that interactions between plasma proteins in blood and the particles (the formation of a biomolecular corona) were mediating some aspects of the particle association with blood immune cells. We therefore performed a "washed blood" assay where all plasma proteins were removed from blood prior to incubation with the polymersomes, as previously described.[37] We found that particle association with blood immune cells was essentially absent when plasma was removed (Figure 5C), demonstrating a dominant effect of plasma proteins on mediating association of polymersomes with blood immune cells. In contrast, the comparator PEG based particles[36] had low but detectable association with blood immune cells in both the presence and absence of plasma illustrating that the low-fouling properties of that system are not influenced as much by plasma proteins. Consistent to our previous observation on different sized polymersome particle associations with cancer cells above (Figure 3), the size of the particles (80 nm versus 400 nm, major axes) did not contribute to any difference in association toward the different types of blood cells (Figure S14, Supporting Information). At the same time, this also suggests that the targeting capacity of the ligands on the polymersome particles were not negated by the presence of PEG units.

3. Conclusion

The concept of a "stealthy" nanoparticle to evade immune cell recognition is a popular avenue for improving the bioavailability of drug carriers. However, these particles tend to lack targeting capabilities. Here in our work, we reported the first synthesis of a selective and multivalent polymersome using two block co-polymers. Using this system, we studied the effect of

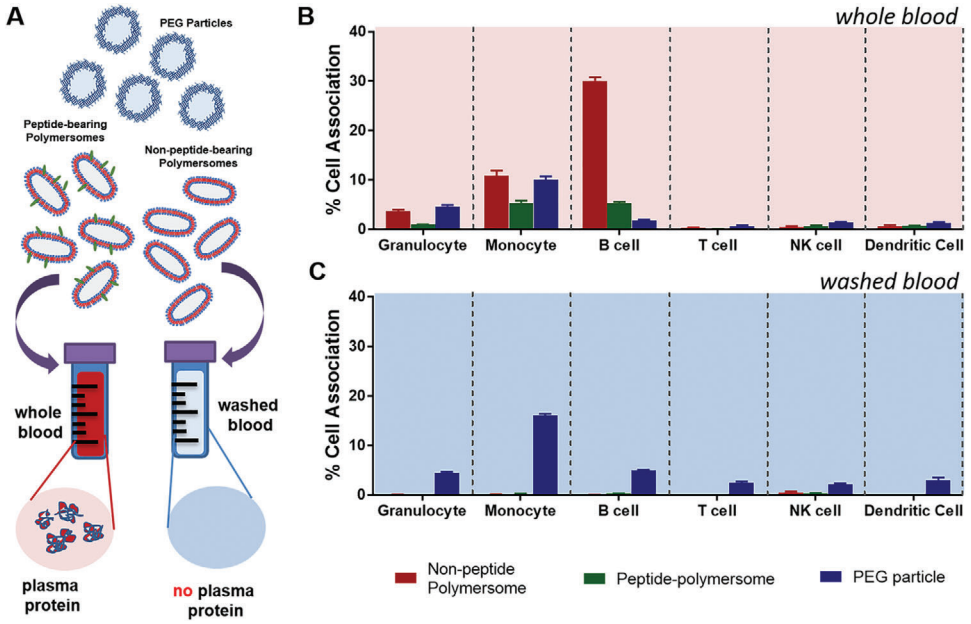

Figure 5. Percentage cell association of small non-peptide bearing and 100% HLD polymersomes to blood cells compared to PEG-based particles. A) Schematic illustration of the experimental setup where the particles were incubated with either a whole blood containing plasma proteins or washed blood with no proteins. B) Graphical representation of the particle association to the whole blood samples. C) Graphical representation of the particle association to washed blood samples. Error bars represent standard error of the mean ($n = 3$).

targeting ligand density on nanoparticle selectivity and stealthiness. We developed an ellipsoidal particle system that has a unique tunable size and shape property with versatile surface functionality. These particles were functionalized with our in-house peptide phage-display cancer cell-targeting peptide, which we showed to effectively target a medulloblastoma cells in vitro. We demonstrated that the particle associated with medulloblastoma cell was modulated by tuning the peptide ligand density on the particles. More importantly, we showed that the effect was, in fact, non-linear. A threshold of ligand density was required to unlock the targeting potential of these particles. Further, these polymersomes also had low levels of association with primary human blood phagocytes. The stealth properties of the polymersomes were improved by including the peptide targeting moiety, an effect that was likely driven by the protective nature of the peptide against binding to blood plasma proteins. Overall, this ellipsoidal polymersome system not only provides valuable insights into ligand design but also is itself a highly promising platform for further development of a selective theranostics for in vivo applications.

4. Experimental Section

Materials: All chemicals were purchased from commercial sources and were used as received unless otherwise stated. Deuterated chloroform was filtered over anhydrous potassium carbonate and neutral aluminum oxide prior to use. Cell lines (DAOY, HEK293, and HBEC5i) used in this study were obtained from American Type Culture Collection (ATCC). Cells were grown in a standard T75 cell culture flask (Corning, USA) and maintained at 37 °C and 4% CO_2 and grown until ≈80–90% confluent. Cells were kept only for 3 months (or before reaches passage 30). For every routine passaging, cells were rinsed with a Dulbecco's phosphate buffered saline (PBS) and harvested by adding Trypsin. Cells were regularly (≈every 3 months) tested for mycoplasma and were negative.

Polymer Synthesis: Synthesis of the Polymer through RAFT Copolymerization: Synthesis of PEG_{43}-*b*-P($NIPAM_{21}$-*co*-*t*-$BocAEA_9$-*co*-PFP_4) by RAFT copolymerization followed the reported procedure by Wong and co-workers with slight modification.[20] NIPAM (438 mg, 3.87 mmol), *t*-BocAEA (300 mg, 1.39 mmol), poly(ethylene glycol) methyl ether 2-(dodecylthiocarbonothioylthio)-2-methyl propionate (PEG_{43}-DDMAT, 351 mg, 0.15 mmol), pentafluorophenol anhydride (128 µL, 0.77 mmol), and 2,2′-azobis(2-methylpropionitrile) (0.2 M in toluene) (155 µL, 0.31 mmol) were dissolved in *N*,*N*-dimethylformamide (1 mL), and degassed by purging with nitrogen for 25 min. The degassed mixture was then placed in a preheated oil bath at 65 °C. After 170 min, the reaction vessel was exposed to air and quenched in an ice bath. The reaction was monitored using ^{19}F NMR, by observing the disappearance of fluorine signal, which indicated the complete exchange of pentafluorophenol group on the polymer backbone. The crude reaction mixture was then diluted in minimal amounts of tetrahydrofuran and precipitated into cold hexane:diethyl ether (2:1, v/v). The resulting precipitate was collected by centrifugation, redissolved in minimal amounts of tetrahydrofuran and precipitated into cold hexane:diethyl ether (2:1, v/v) again. The purification process was repeated four times in total. The purified product was collected and dried under high vacuum to yield PEG_{43}-*b*-P($NIPAM_{21}$-*co*-*t*-$BocAEA_9$-*co*-PFP_4) as a light yellow solid (943.9 mg). The number of NIPAM and *t*-BocAEA repeating units in the diblock terpolymer were determined using NMR ($CDCl_3$) (see Figure S1, Supporting Information). $M_{n,\,GPC} = 13\,800$ g mol^{-1}; $M_{n,\,NMR} = 9336$ g mol^{-1}; $Đ = 1.06$.

Polymer Synthesis—Peptide Conjugation and Capping Step (LLD Polymer): PEG_{43}-*b*-P($NIPAM_{21}$-*co*-*t*-$BocAEA_9$-*co*-PFP_4) (300 mg, 1 equiv.), FSRPAFL peptide[22] (36 mg, 1.5 equiv.), and diisopropylethylamine (100 µL, excess) were dissolved in peptide-grade *N*,*N*-dimethylformamide (4 mL) and stirred for 2 days at 40 °C under nitrogen flow. The reaction mixture was then dialyzed in a mixture of dichloromethane/ethanol (1:1). Solvents were replaced three times after stirring for at least 2 h. The product was recovered after dialysis (3500 MWCO) and dried in vacuo to afford dry yellow oil (281.1 mg). Since the ^{19}F NMR spectra (see Figure 1) indicated that there were still some unreacted polymer, crude product was redissolved in *N*,*N*-dimethylformamide (4 mL), along with more peptide (31 mg), and diisopropylethylamine (1 mL), and stirred at 40 °C under nitrogen flow for another 24 h. A reduction in the fluorine signal

was observed. Propargylamine (15 µL, 6 equiv.) was then added to the reaction mixture to react all unreacted pentafluorophenyl groups for 24 h. The disappearance in polymer-bound fluorine signal (broad, Figure 1) indicated that the polymer-bound pentafluorophenyl group has been fully substituted. The reaction was then stopped and precipitated onto hexane/ether (1:1), centrifuged, and dried in vacuo. The product was dialyzed in dichloromethane/ethanol (1:1; v/v). Yellow pale solid (292 mg) PEG_{43}-*b*-P($NIPAM_{21}$-*co*-*t*-$BocAEA_9$-*co*-$peptide_{1.5}$) was obtained after drying in vacuo.

Polymer Synthesis—Tert-Butyloxycarbonyl (t-Boc)-Deprotection and PDMI-PFP Conjugation (LLD polymer): PEG_{43}-*b*-P($NIPAM_{21}$-*co*-*t*-$BocAEA_9$-*co*-$FSRPAFL_{1.5}$) (100 mg) was dissolved in dichloromethane/trifluoroacetic acid (1:1, v/v, 12 mL) was added to the solution drop wise on an ice bath. Stirring then continued at room temperature for 3 h. The complete deprotection of *t*-Boc was confirmed by ^{1}H NMR. After 3 h, the reaction mixture was dried and washed azeotropically using dichloromethane (5 × 6 mL) to remove the residual acid. After final drying in vacuo, PEG_{43}-*b*-P($NIPAM_{21}$-*co*-AEA_9-*co*-$peptide_{1.5}$) was obtained as a pale yellow solid (128 mg). PEG_{43}-*b*-P($NIPAM_{21}$-*co*-AEA_9-*co*-$peptide_{1.5}$) (50 mg) and PDMI-PFP (43 mg) were suspended in peptide-grade *N*,*N*-dimethylformamide (5 mL). Diisopropylethylamine (1 mL) was then added to the suspension and stirred at 40 °C under nitrogen flow. After 2 days, the crude reaction mixture was purified using size exclusion chromatography with *N*,*N*-dimethylformamide as the eluent. The product was then dialyzed in dichloromethane/ethanol (1:1, v/v). The product was then concentrated in vacuo to afford red solid (12.3 mg). ^{1}H–^{13}C HSQC NMR spectrum of PEG_{43}-*b*-P($NIPAM_{21}$-*co*-$PDMI_9$-*co*-$peptide_{1.5}$) was obtained using dimethylformamide-d_6 (see Figure S3, Supporting Information). $M_{n,\,GPC}$ = 18 300 g mol^{-1}; $M_{n,\,NMR}$ = 12 680 g mol^{-1}; $Đ$ = 1.16.

Polymer Synthesis—Peptide Conjugation (HLD Polymer): PEG_{43}-*b*-P($NIPAM_{21}$-*co*-*t*-$BocAEA_9$-*co*-PFP_4) (125 mg, 1 equiv.), FSRPAFL peptide (114 mg, 6 equiv.), and diisopropylethylamine (100 µL, excess) were dissolved in peptide-grade *N*,*N*-dimethylformamide (5 mL) and stirred for 3 days at 40 °C under nitrogen flow. The reaction mixture was then dialyzed in a mixture of dichloromethane/ethanol (1:1). Solvents were replaced three times after stirring for at least 2 h. The product was recovered after dialysis and dried in vacuo to afford PEG_{43}-*b*-P($NIPAM_{21}$-*co*-*t*-$BocAEA_9$-*co*-$peptide_4$) as a yellow oil (201 mg). $M_{n,\,GPC}$ = 17 800 g mol^{-1}; $M_{n,\,NMR}$ = 9336 g mol^{-1}; $Đ$ = 1.01.

Polymer Synthesis—Tert-butyloxycarbonyl (t-Boc)-Deprotection and PDMI-PFP Conjugation (HLD Polymer): PEG_{43}-*b*-P($NIPAM_{21}$-*co*-*t*-$BocAEA_9$-*co*-$FSRPAFL_4$) (201 mg) was dissolved in dichloromethane/trifluoroacetic acid (1:1, v/v, 12 mL) was added to the solution dropwise on an ice bath. Stirring then continues at room temperature for 3 h. The complete deprotection of *t*-Boc was confirmed by ^{1}H NMR. After 3 h, the reaction mixture was dried and washed azeotropically using dichloromethane (5 × 6 mL) to remove the residual acid. After final drying in vacuo, PEG_{43}-*b*-P($NIPAM_{21}$-*co*-AEA_9-*co*-$peptide_4$) was obtained as a pale yellow solid (185 mg). PEG_{43}-*b*-P($NIPAM_{21}$-*co*-AEA_9-*co*-$peptide_4$) (97 mg) and PDMI-PFP (71 mg) were suspended in peptide-grade *N*,*N*-dimethylformamide (10 mL). Diisopropylethylamine (0.1 mL) was then added to the suspension and stirred at 40 °C under nitrogen flow. After 2 days, the crude reaction mixture was purified using size exclusion chromatography with *N*,*N*-dimethylformamide as the eluent. The product was then dialyzed in dichloromethane/ethanol (1:1, v/v). The PEG_{43}-*b*-P($NIPAM_{21}$-*co*-$PDMI_9$-*co*-$peptide_4$) product was then concentrated in vacuo to afford red solid (200 mg). $M_{n,\,GPC}$ = 18 920 g mol^{-1}; $M_{n,\,NMR}$ = 12 678 g mol^{-1}; $Đ$ = 1.02.

Polymersome Formation: In a typical experiment, a 4 mL sample tube equipped with a magnetic stir bar (2.5 mm length × 5 mm width) was charged with 0.5 mg of PEG_{43}-*b*-P($NIPAM_{21}$-*co*-$PDMI_9$) and PEG_{43}-*b*-P($NIPAM_{21}$-*co*-*t*-$BocAEA_9$-*co*-$peptide_{1.5/4}$).[20] Stock solution of PEG_{43}-*b*-P($NIPAM_{21}$-*co*-$PDMI_9$) was prepared using neat tetrahydrofuran, while polymer was first dissolved in *N*,*N*-dimethylformamide (10% (v/v) of final volume) before addition of tetrahydrofuran. Small polymersomes populations were formed by using 500 µL of total tetrahydrofuran (or 10% (v/v) *N*,*N*-dimethylformamide in tetrahydrofuran), while large polymersomes were formed using 800 µL of the organic solvents. Gentle shaking was applied to homogenize the solution before water (500 µL) was added directly into the polymer solution in a single portion. The mixture was then stirred at room temperature in the fume hood (100 rpm) to allow the evaporation of tetrahydrofuran (≈16–20 h). Samples containing polymer were dialyzed against water to remove *N*,*N*-dimethylformamide from the polymersome solutions.

Synthesis of PEG Particles: PEG particles were prepared based on a mesoporous silica (MS) templating method according to a previous protocol.[23,36,38] MS templates with an average size of 400 nm were synthesized using polyelectrolyte-surfactant complexes as templates according to a previously reported method.[39] For fluorescence labeling, PEG particles were labeled with AF647. The number of particles were counted by flow cytometry (Apogee A50-Micro flow cytometer, UK) before adding to cells.

Transmission Electron Microscopy: TEM measurements were carried out on an FEI Tecnai G2 20 TEM operating at an accelerating voltage of 200 kV. Images were acquired using a BM Eagle 2K CCD Camera. Samples were prepared by dropping 10 µL of polymersome solution (0.2 mg mL^{-1}) onto a formvar-coated carbon grid. The drop was immediately blotted with a pre-cut filter paper to leave behind a thin film of sample before being dried using a gentle stream of nitrogen. No staining was used.

Cytotoxicity Studies: In order to assess the biocompatibility of these polymersomes, cytotoxicity profiles of the particles were determined using AlamarBlue Assay. DAOY cells in high-glucose Dulbecco's modified Eagle medium (DMEM) containing 10% fetal bovine serum and L-glutamine (1000 cells per 100 µL) were seeded into 96-multiwell tissue culture plates and allowed to adhere overnight. The following day, polymersomes of 0.025 mg mL^{-1}, 2.5 µg mL^{-1}, 0.25 µg mL^{-1}, 25 ng mL^{-1}, and 2.5 ng mL^{-1} concentrations were prepared by dissolving the stock solution (1 mg mL^{-1}) in DMEM. After removal of cell media, the polymersome solutions (100 µL) were pipetted onto the wells in triplicate. A solution of cell culture media devoid of any polymersomes serves as a control. The cells were incubated at 37 °C with 5% CO_2. 72 h post-treatment the polymersomes were removed and replaced with fresh alamarBlue reagent (10% in DMEM cell culture media). The cells were incubated for another 6 h at 37 °C with 5% CO_2 before subjected to fluorometric measurements using a microplate spectrophotometer at 570 nm (reference wavelength 595 nm). IC50 values were calculated using GraphPad Prism 7 (see Figure S8, Supporting Information). Since the highest tested concentration for the HLD polymersomes was toxic for the cells at 72 h, the test was repeated with a 2 h incubation. Results from this test indicated that the cells were viable at this time point (see Figure S8C, Supporting Information).

Flow Cytometry: Cellular uptake of the polymersomes was assessed using a flow cytometry as previously described.[22] Cells in DMEM media (DAOY 200 000 cells per mL) were seeded onto a 6-well tissue culture plates and allowed to adhere overnight. The following day, the cell culture media was replaced with polymersomes solutions (0.05 mg mL^{-1}) that were prepared by diluting the stock solutions (1 mg mL^{-1}) with cell culture media. The cells were incubated at either 37 °C with 5% CO_2 or 4 °C in a cold room. After 2 h, the treatment solutions were removed and the cells were washed with PBS (1 mL). After aspiration of PBS, cells were treated with Trypsin (2 mL) for 2 min, neutralized with PBS (4 mL), and centrifuged for 1 min (1200 rpm). After removal of the supernatant, cells were re-suspended into PBS containing 2 mM of ethylenediaminetetraacetic acid (EDTA) and 2% fetal bovine serum (350 µL). Cell uptake was measured using BD FACSCanto benchtop cell analyzer. Percentage cellular uptake was calculated and graphed using GraphPad Prism 7 (see Figure S11, Supporting Information).

Confocal Microscopy: Cellular uptake of the polymersomes in medulloblastoma cells was investigated using live cell imaging microscopy technique. Confocal microscope analyses were performed on a Zeiss 880, equipped with a 63.0 × 1.40 NA oil immersion objective. Fluorescence images were recorded using a 488 laser with a detector wavelength range of 493–674 nm. Image processing was performed with FIJI, an open source image processing package based on ImageJ. Cells in culture media (DAOY 20 000 cells per mL) were seeded onto a 6-well glass-bottom tissue culture plate (20 mm) and allowed to adhere overnight. Cells were

incubated with 0.025 mg mL^{-1} of polymersome samples (a concentration that was confirmed to be non-toxic toward the cells, (see Figure S10, Supporting Information) for 2 h and imaged on a confocal microscope. An increase in particle uptake was observed after a longer incubation period of 4- and 8-h (data not shown). For the purpose of this study, 2 h period was selected as both a convenient time point as well as to ensure that the measured cellular uptake was not a result of particle oversaturation. The images in Figure S10, Supporting Information, showed that all of the polymersome samples were taken up by the cell and internalized into the cytosolic compartment (red). Minimal localization inside the nucleus was observed as indicated by the hollow appearance in the center of the cells (Figure S10, Supporting Information). A similar cellular uptake profile was observed across all the samples regardless of peptide functionalization.

Human Blood Preparation: Fresh whole blood was collected from a healthy human donor after obtaining informed consent in accordance with The University of Melbourne Human Research Ethics approval (No. 1 443 420) and the Australian National Health and Medical Research Council Statement on Ethical Conduct in Human Research. Blood was drawn by venepuncture into Vacuette collection tubes containing sodium heparin (Greiner Bio-One) and gently inverted five times. Cell counts were obtained using a CELL-DYN Emerald analyzer (Abbott). To prepare washed blood, 3 mL whole blood was topped up with 47 mL PBS and centrifuged at 950 × *g* for 10 min, slow brake. The supernatant was removed and this wash step was repeated five times. The absence of plasma proteins was confirmed by the lack of absorbance of the supernatant at 280 nm (Nanodrop 2000, ThermoFisher Scientific, Australia). Blood cells were resuspended in serum-free RPMI 1640 media (ThermoFisher) at the same cell concentration as whole blood.

Blood Association Assay: Whole or washed blood (100 µL) was introduced into FACS tubes and incubated at 37 °C for 10 min according to previously reported method.[37] Small polymersomes (non-peptide bearing and 100% HLD) were added directly at 1 µg mL^{-1} concentration and incubated for 1 h at 37 °C, before placing all tubes on ice. Erythrocytes were lysed with 1X Pharm Lyse buffer (BD Biosciences). WBCs were pelleted (500 g, 7 min.) and washed twice with PBS. Cells were phenotyped on ice (1 h) using optimized concentrations of fluorescently tagged antibodies to identify the following white cell populations: T cells (antibody CD3- AF700, BD Biosciences, clone SP34-2), monocytes (antibody CD14-APC-H7 BD Biosciences, clone MϕP9), neutrophils (antibody CD66b-BV421, BD Biosciences, clone G10F5), B cells (antibody CD19-BUV395, BD Biosciences, clone SJ25C1), NK cells (antibody CD56-PE, BD Biosciences, clone B159), and a cocktail of antibodies to identify dendritic cells (lineage-1 FITC antibodies BD Biosciences and HLA-DR PE-CF594 antibody, BD Biosciences, clone G46-6). The stained cells were washed twice in cold (4 °C) PBS/2 mM EDTA/0.5% BSA, and fixed (1% v/v formaldehyde in PBS). The subpopulations of white blood cells associating with the perylene-labeled polymersomes was measured by flow cytometry (LSRFortessa, BD Biosciences) and analyzed using FlowJo V10 with cell types identified using the gating strategy shown in Supporting Information (see Figure S15, Supporting Information).

Statistical Analysis: The statistical two-way ANOVA (repeated measures with both factors) analysis reported in this manuscript was generated using GraphPad Prism version 7 for Windows, GraphPad Software, San Diego California USA (www.graphpad.com). This statistical analysis was performed for all the flow cytometry cellular association experiments that utilized a Tukey's multiple comparison test. Error bars presented in the figures were reflective of the standard error of the mean based on three independent measurements collected for each individual parameter. Significance was presented in terms of *p* values, which denoted the confidence interval of the differences between two means.

Supporting Information

Supporting Information is available from the Wiley Online Library or from the author.

Acknowledgements

M.K., F.C., S.J.K, and P.T. were in part supported by the Australian Research Council Centre of Excellence in Convergent Bio-Nano Science and Technology (project number CE140100036) which also provided a PhD scholarship to K.T. This work was supported by grants from the Ross Trust Foundation (J.A.M.) and Steadfast Foundation (J.A.M.). J.A.M. was in part supported by funding from the Olivia Lambert Foundation. F.C. acknowledges the award of a National Health and Medical Research Council Senior Principal Research Fellowship (GNT1135806). The authors thank the staff of Mark Wainwright Analytical Centre at UNSW.

Conflict of Interest

The authors declare no conflict of interest.

Keywords

cancer drug delivery, multivalency, nanomedicines, peptides, polymeric nanoparticles, targeting ligands

Received: February 17, 2020
Revised: April 20, 2020
Published online:

[1] Y. Barenholz, *J. Controlled Release* **2012**, *160*, 117.
[2] W. J. Gradishar, *Expert Opin. Pharmacother.* **2006**, *7*, 1041.
[3] K. Maier-Hauff, F. Ulrich, D. Nestler, H. Niehoff, P. Wust, B. Thiesen, H. Orawa, V. Budach, A. Jordan, *J. Neuro-Oncol.* **2011**, *103*, 317.
[4] D. Bobo, K. J. Robinson, J. Islam, K. J. Thurecht, S. R. Corrie, *Pharm. Res.* **2016**, *33*, 2373.
[5] A. M. Alkilany, L. Zhu, H. Weller, A. Mews, W. J. Parak, M. Barz, N. Feliu, *Adv. Drug Delivery Rev.* **2019**, *143*, 22.
[6] H. Lee, T. W. Odom, *Nanomedicine* **2015**, *10*, 177.
[7] D. R. Elias, A. Poloukhtine, V. Popik, A. Tsourkas, *Nanomed.: Nanotechnol., Biol. Med.* **2013**, *9*, 194.
[8] X. Zhu, C. Vo, M. Taylor, B. R. Smith, *Mater. Horiz.* **2019**, *6*, 1094.
[9] L. Florez, C. Herrmann, J. M. Cramer, C. P. Hauser, K. Koynov, K. Landfester, D. Crespy, V. Mailänder, *Small* **2012**, *8*, 2222.
[10] S. Dasgupta, T. Auth, G. Gompper, *Nano Lett.* **2014**, *14*, 687.
[11] P. Decuzzi, M. Ferrari, *Biophys. J.* **2008**, *94*, 3790.
[12] S. Barua, J. Yoo, P. Kolhar, A. Wakankar, Y. R. Gokarn, S. Mitragotri, *Proc. Natl. Acad. Sci. USA* **2013**, *110*, 3270.
[13] J. S. Lee, J. Feijen, *J. Controlled Release* **2012**, *161*, 473.
[14] R. P. Brinkhuis, F. P. J. T. Rutjes, J. C. M. Van Hest, *Polym. Chem.* **2011**, *2*, 1449.
[15] L. Messager, J. Gaitzsch, L. Chierico, G. Battaglia, *Curr. Opin. Pharmacol.* **2014**, *18*, 104.
[16] C. K. Wong, A. D. Martin, M. Floetenmeyer, R. G. Parton, M. H. Stenzel, P. Thordarson, *Chem. Sci.* **2019**, *10*, 2725.
[17] C. K. Wong, M. H. Stenzel, P. Thordarson, *Chem. Soc. Rev.* **2019**, *48*, 4019.
[18] R. S. M. Rikken, H. Engelkamp, R. J. M. Nolte, J. C. Maan, J. C. M. van Hest, D. A. Wilson, P. C. M. Christianen, *Nat. Commun.* **2016**, *7*, 12606.
[19] S. Keshavan, P. Calligari, L. Stella, L. Fusco, L. G. Delogu, B. Fadeel, *Cell Death Dis.* **2019**, *10*, 569.
[20] C. K. Wong, A. F. Mason, M. H. Stenzel, P. Thordarson, *Nat. Commun.* **2017**, *8*, 1240.

[21] Z. Chen, V. Stepanenko, V. Dehm, P. Prins, L. D. A. Siebbeles, J. Seibt, P. Marquetand, V. Engel, F. Würthner, *Chem. - Eur. J.* **2007**, *13*, 436.
[22] K. C. Tjandra, N. McCarthy, L. Yang, A. J. Laos, G. Sharbeen, P. A. Phillips, H. Forgham, S. M. Sagnella, R. M. Whan, M. Kavallaris, P. Thordarson, J. A. McCarroll, *J. Med. Chem.* **2020**, *63*, 2181.
[23] M. Hu, S. Alcantara, J. J. Richardson, K. Liang, R. I. Price, J. Cui, R. De Rose, B. M. Paterson, Y. Yan, K. Alt, S. J. Kent, P. S. Donnelly, K. Peter, F. Caruso, C. M. Jeffery, C. E. Hagemeyer, *ACS Nano* **2015**, *9*, 1571.
[24] J. Nicolas, S. Liu, D. Zhao, F. Caruso, E. Reichmanis, J. M. Buriak, *Chem. Mater.* **2018**, *30*, 6587.
[25] J. Chiefari, Y. K. Chong, F. Ercole, J. Krstina, J. Jeffery, T. P. T. Le, R. T. A. Mayadunne, G. F. Meijs, C. L. Moad, G. Moad, E. Rizzardo, S. H. Thang, *Macromolecules* **1998**, *31*, 5559.
[26] J. Du, Y. Chen, *Macromolecules* **2004**, *37*, 5710.
[27] H. R. Marsden, L. Gabrielli, A. Kros, *Polym. Chem.* **2010**, *1*, 1512.
[28] S. Bhattacharjee, *J. Controlled Release* **2016**, *235*, 337.
[29] L. Hunt, D. L. Hacker, F. Grosjean, M. De Jesus, L. Uebersax, M. Jordan, F. M. Wurm, *Biotechnol. Bioeng.* **2005**, *89*, 157.
[30] L. Mocé-Llivina, J. Jofre, *Cytotechnology* **2004**, *46*, 57.
[31] G. Shaw, S. Morse, M. Ararat, F. L. Graham, *FASEB J.* **2002**, *16*, 869.
[32] K. C. Tjandra, P. Thordarson, *Bioconjugate Chem.* **2019**, *30*, 503.
[33] F. J. Martinez-Veracoechea, D. Frenkel, *Proc. Natl. Acad. Sci. USA* **2011**, *108*, 10963.
[34] T. Curk, J. Dobnikar, D. Frenkel, in *Multivalency Concepts, Research and Applications* (Eds: J. Huskens, L. J. Prins, R. Haag, B. J. Ravoo), Wiley, Chichester, UK **2017**, pp. 75–101.
[35] A. C. G. Weiss, H. G. Kelly, M. Faria, Q. A. Besford, A. K. Wheatley, C. S. Ang, E. J. Crampin, F. Caruso, S. J. Kent, *ACS Nano* **2019**, *13*, 4980.
[36] J. Cui, Y. Ju, Z. H. Houston, J. J. Glass, N. L. Fletcher, S. Alcantara, Q. Dai, C. B. Howard, S. M. Mahler, A. K. Wheatley, R. De Rose, P. T. Brannon, B. M. Paterson, P. S. Donnelly, K. J. Thurecht, F. Caruso, S. J. Kent, *Adv. Healthcare Mater.* **2019**, *8*, 1801607.
[37] J. J. Glass, L. Chen, S. Alcantara, E. J. Crampin, K. J. Thurecht, R. De Rose, S. J. Kent, *ACS Macro Lett.* **2017**, *6*, 586.
[38] J. Cui, K. Alt, Y. Ju, S. T. Gunawan, J. A. Braunger, T. Y. Wang, Y. Dai, Q. Dai, J. J. Richardson, J. Guo, M. Björnmalm, C. E. Hagemeyer, F. Caruso, *Biomacromolecules* **2019**, *20*, 3592.
[39] J. G. Wang, H. J. Zhou, P. C. Sun, D. T. Ding, T. H. Chen, *Chem. Mater.* **2010**, *22*, 3829.